Max-Planck-Institut für Kohlenforschung

Journal article published in: J. Chem. Theory Comput. 2017, 13, 6, 2954-2961

https://pubs.acs.org/doi/abs/10.1021/acs.jctc.7b00016t

Importance of MM Polarization in QM/MM Studies of Enzymatic Reactions: Assessment of the QM/MM Drude Oscillator Model

*Abir Ganguly, Eliot Boulanger and Walter Thiel**

Max-Planck-Institut für Kohlenforschung, Kaiser-Wilhelm-Platz 1, 45470 Mülheim an der Ruhr, Germany

Keywords: Polarization, free energy simulations, chorismate mutase, p-hydroxybenzoate hydroxylase

ABSTRACT: For accurate quantum mechanics/molecular mechanics (QM/MM) studies of enzymatic reactions, it is desirable to include MM polarization, for example by using the Drude oscillator (DO) model. For a long time, such studies were hampered by the lack of well-tested polarizable force fields for proteins. Following up on a recent preliminary QM/MM-DO assessment (*J. Chem. Theory. Comput.* **2014**, *10*, 1795-1809) we now report a comprehensive investigation of the effects of MM polarization on two enzymatic reactions, namely the Claisen rearrangement in chorismate mutase and the hydroxylation reaction in p-hydroxybenzoate hydrolase, using the QM/CHARMM-DO model and two QM methods (B3LYP, OM2). We compare the results from extensive geometry optimizations and free energy simulations at the QM/MM-DO level to those obtained from analogous calculations at the conventional QM/MM level.

1. Introduction

Quantum mechanics/molecular mechanics (QM/MM) approaches have emerged as the method of choice for modeling enzymatic processes. They have been applied with great success to obtain qualitative insights into reaction mechanisms and to provide quantitative predictions of observables for comparison with experiment.[1-6] QM/MM calculations of enzymatic reactions commonly treat the QM region with first-principles methods, while describing the MM region by a classical additive force field. One of the approximations in this standard QM/MM formalism is the use of a fixed-point charge representation of the MM atoms offered by the additive MM force fields. There is evidence that inclusion of MM polarization effects induced by the QM electron density can be important in the QM/MM treatment of enzymatic reactions, particularly if the reaction involves negatively charged or very polar species.[5]

Efforts to include explicit polarization at the MM level have been ongoing since the pioneering QM/MM model study of Warshel and Levitt in 1976,[7] in which MM polarization was incorporated using a point dipole approach. Over the next decades, several other treatments of MM polarization have been proposed, including techniques based on induced dipoles,[8-12] fluctuating charges,[13-15] and Drude oscillators (DOs).[16-21] In the latter approach, adopted in this study, a mobile charge, referred to as the Drude particle (DP), is connected to a polarizable MM atom by means of a short harmonic spring. The total charge of the MM atom-DP pair is conserved by placing an equal and opposite charge on the MM nucleus. The MM atom-DP dipole thus created responds to changes in the electrostatic environment of the MM atom, thus giving rise to polarization.

In the past, QM/MM studies with polarizable MM regions were performed with

special-purpose polarizable protein force fields. Apart from the pioneering work of Warshel and Levitt,[7] we note that Illingworth et al. used an induced-charge model of MM polarization[22] to study the Claisen rearrangement catalyzed by chorismate mutase;[23] they reported a significant lowering of the total energy of the stationary points upon inclusion of MM polarization, but the energy barrier of the reaction remained essentially unchanged since the reactant and transition state were equally stabilized. Systematic QM/MM studies of the effect of MM polarization in enzymatic reactions have been hindered by the lack of well-tested polarizable force fields (PFFs) for proteins. Over the past few years, the intense efforts in the area of PFF development have led to the release of highly optimized PFFs, such as the AMOEBA force field[12] based on dynamically fluctuating charges and the CHARMM-DO force field based on the DO model.[24]

The DO model is particularly suited for QM/MM implementation as it retains the point charge description of an additive MM force field. In our laboratory we have implemented the DO model into the QM/MM framework, initially using the GROMOS charge-on-spring force field,[25] and more recently using the CHARMM-DO force field.[26,27] We have reported a preliminary assessment of the QM/CHARMM-DO model for the reactions catalyzed by the enzymes chorismate mutase (CM) and p-hydroxybenzoate hydroxylase (PHBH) based on QM/MM-DO single-point calculations at QM/MM-optimized geometries, which indicated that MM polarization affects the energy barrier by 5-15% in CM and 5-20% in PHBH.[26,27]

In this study, we perform a more comprehensive examination of the effects of MM polarization in QM/MM studies of enzymatic reactions, again using the CM- and PHBH-catalyzed reactions as representative examples. We generate potential energy

profiles and free energy profiles for these catalytic reactions through exhaustive geometry optimizations and free energy simulations, respectively. We compare the results obtained with the QM/MM-DO model to those obtained from analogous calculations with the conventional QM/MM model. For both enzymes, inclusion of MM polarization leads to an increase in the computed energy and free energy barriers, which is more pronounced for PHBH than CM, presumably because the PHBH-catalyzed reaction involves significant charge transfer. To our knowledge, these findings offer the first systematic assessment of PFF effects in QM/MM studies of enzymatic reactions.

2. Methods

The theory underlying the Drude model and the details of its implementation in a QM/MM framework have been described previously.[26,27] Here we only recapitulate the main features. The classical Drude model aims at simulating electronic polarizability at MM level.[16] It consists of adding two equal and opposite charges to every polarizable atom, one of which is positioned at the atomic nucleus, while the other, referred to as the Drude particle (DP), is linked to the atom by a short harmonic spring, and is free to move.[21,28] The induced atomic dipole, μ, is expressed as

$$\mu = \alpha E$$

where E is the electric field and α is the atomic polarizability, which is related to the charge on the DP, q, and the force constant, k, of the spring according to

$$\alpha = \frac{q^2}{k}$$

In additive force fields, the 1,2 and 1,3 nonbonded interactions are typically ignored, while 1,4 interactions are often scaled to reproduce correct electrostatics.[29,30] For PFFs, the 1,2 and 1,3 induced dipole interactions are crucially important for obtaining proper molecular polarizabilities.[24] In the CHARMM-DO force field, these interactions are taken into account using the Thole approach.[31] The force field also has provisions for lone pairs (LPs), which not only provides a better description of the fixed charge distribution, but also allows the modeling of anisotropic polarizability.[32] LPs are represented as additional point charges that are rigidly linked to the polarizable atoms.

In the QM/MM framework, the DPs and LPs are incorporated in the QM computations in a similar fashion as standard MM point charges; i.e. by adding one-electron integral terms to the QM Hamiltonian.[25-27] To simultaneously converge the DP positions and the QM energy, a dual self-consistent field (SCF) approach is employed that includes the following: (a) a full QM computation in the fixed field of MM point charges, DPs and LPs; (b) updating the DP positions based on the QM wave function; and (c) iterating between (a) and (b) until the QM energy and the DP positions are converged with respect to each other.[26,27]

3. Computational Details

The potential energy profiles for the CM- and PHBH-catalyzed reactions were obtained using both the QM/MM-DO model and the conventional additive QM/MM model; the latter will be labeled as QM/MM-ADD in the following to avoid confusion. The energy profiles were calculated through extensive geometry optimizations along suitably chosen reaction coordinates (see Results section and Supporting Information for further details).

The optimizations were performed in hybrid delocalized internal coordinates using the HDLCOpt optimizer available in ChemShell.[33]

The free energy simulations for the CM- and PHBH-catalyzed reactions were carried out using a recently developed enhanced sampling technique, the finite temperature string method.[34] The underlying theory and applications of this method have been detailed in several recent studies.[35-38] Hence we outline the method only briefly here. A reaction pathway is approximated as a curve passing through the reduced dimensions of a few important reaction coordinates (RCs) that characterize the reaction. Starting from an initial guess, the curve is divided into a series of equally spaced images, each of which corresponds to certain specific values of the RCs. At each image, short trajectories are propagated with the RCs harmonically restrained to their current values. The positions of the images are updated based on the mean values of the RCs calculated from the respective MD trajectories, and a new curve is constructed connecting the new images. This procedure of updating the curve based on restrained dynamics is repeated until convergence is achieved, that is when the RMSD between the curves from successive iterations has dropped below a certain threshold. Finally, the restrained MD trajectories for all the images from the various iterations are jointly unbiased to generate the *M*-dimensional free energy surface underlying the reaction, where *M* is the number of RCs considered. The converged curve represents the minimum free energy path (MFEP) of the reaction in the *M*-dimensional phase space.

Application of the string method is computationally expensive, particularly in the QM/MM framework. To limit the computational effort we adopted the following strategy: The MFEPs of the CM and PHBH catalytic reactions were first calculated using

the string method and the QM/MM-ADD model. Thereafter one-dimensional umbrella sampling (US) simulations were performed along these MFEPs with the QM/MM-DO and QM/MM-ADD models to obtain the final free energy profiles. The underlying assumption is that the qualitative mechanism of the reaction is not affected by the inclusion of MM polarization. Additional detailed information on the string calculations and the US simulations is provided in the Supporting Information.

All QM/MM calculations were carried out using the ChemShell software package.[39-41] We applied two different QM methods: density functional theory (DFT) using the hybrid functional B3LYP[42,43] with the def2-SVP basis set,[44] and the semiempirical OM2 method.[45-47] The QM energies and gradients were computed at these levels using the Turbomole[48] and MNDO[49] programs, respectively. Additive MM terms were calculated using the DL-POLY[50] program and the CHARMM22 force field.[51] DO-related computations were performed using a separate hybrid module in ChemShell implemented recently in our group. The polarizable MM region was described by the CHARMM-DO force field for proteins[24] and the SWM4-NDP model for water.[52] In the following section, we focus on the results from the DFT/MM calculations, while those from analogous OM2/MM calculations are documented in the Supporting Information.

4. Results

4.1 Chorismate Mutase

In the CM active site a relatively small substrate, chorismate (CHO), is non-covalently bound to the protein, which makes this enzyme an ideal subject for QM/MM tests. During

the catalytic reaction, CHO is converted to prephenate through a Claisen rearrangement (Scheme 1). CM has been the focus of several experimental and theoretical studies and its reaction mechanism is well understood.[1] The transformation of CHO to prephenate involves negligible charge transfer, and thus QM/MM calculations of this reaction are expected to be rather insensitive towards MM polarization.

In this study we considered five random solvent-equilibrated snapshots of CM available from a previous study in our group.[53] The QM region consisted of CHO, while the rest of the system was described either at the MM-ADD or MM-DO level. All atoms lying outside a residue-based cutoff of 10 Å from the C1 atom of CHO were held fixed at their initial coordinates. The non-bonded parameters of the substrate were borrowed from the CHARMM22 force field as in our previous study.[27] The potential energy profiles of the catalytic reaction were determined by performing PES scans along a reaction coordinate describing the bond forming and bond breaking processes, namely the difference between the C9-O8 and C1-C13 distances in CHO (Scheme 1).

$$z = d(C9 - O8) - d(C1 - C13)$$

The scans were performed with a grid spacing of 0.25 Å and were repeated multiple times, driving the reaction in both forward and backward directions, until the energy profiles obtained in both directions were identical.

The reaction energies (ΔE) and activation energies ($\Delta E^{\ddagger}$) of the CM-catalyzed reaction calculated using the DFT/MM-DO and DFT/MM-ADD models are listed in Table 1 for the five selected snapshots; the corresponding potential energy profiles for snapshot 1 are illustrated in Figure 1A. The average barrier $\Delta E^{\ddagger}$ obtained with the DFT/MM-ADD model is close to the experimental value of 12.7 kcal/mol.[54] Upon

inclusion of MM polarization at the DFT/MM-DO level, snapshots 1 and 3-5 exhibit a modest increase in both ΔE and $\Delta E^{\ddagger}$, by 0.4-2.6 kcal/mol (2-20%) and 0.5-1.3 kcal/mol (5-8%), respectively; for snapshot 2, ΔE remains unaffected while $\Delta E^{\ddagger}$ decreases slightly (by 0.4 kcal/mol). Analogous calculations at the OM2/MM-ADD and OM2/MM-DO levels show very similar trends (Table S1). The similarity of the energy profiles obtained with the QM/MM-DO and QM/MM-ADD models is in line with the fact that the corresponding optimized geometries of the stationary points are also very similar (Table S2). The root-mean-square deviations (RMSDs) between DFT/MM-DO and DFT/MM-ADD optimized geometries for reactant, transition state, and product are well below 0.2 Å for all snapshots.

Free energy profiles of the CM-catalyzed reaction calculated using the DFT/MM-DO and DFT/MM-ADD models are illustrated in Figure 1B, and numerical results for free energies and geometric RMSDs are listed in Table 2. The reaction coordinate used for the US simulations was identical to that used to obtain the potential energy profiles. According to Figure 1B and Table 2, the free energy barrier ($\Delta G^{\ddagger}$) of the reaction at the DFT/MM-ADD level is 14.1 kcal/mol. This number is in close agreement with the experimentally measured value of 15.4 kcal/mol.[54] The profile obtained from the DFT/MM-DO model is shifted somewhat upwards, with an increase of 2.5 kcal/mol in $\Delta G^{\ddagger}$ and of 2.9 kcal/mol in the reaction free energy (ΔG), compared with DFT/MM-ADD. This change is in the same direction as in the case of the energy profiles (Table 1) but is somewhat more pronounced. The DFT/MM-DO calculated free energy profile also features a shifted reactant minimum, which is reflected in the high RMSD between the average reactant state geometries sampled in the QM/MM-DO and QM/MM-ADD US

simulations (Table 2). QM/MM-DO favors a more open CHO geometry with an increased C1-C13 distance (Figure 1C). The RMSDs between the average transition state and product geometries sampled in the QM/MM-DO and QM/MM-ADD US simulations are rather low, suggesting that MM polarization does not strongly affect these states (Figures 2D and 2E). Thus, inclusion of MM polarization at the DFT/MM-DO level preferentially stabilizes the reactant state, which in turn causes a slight increase in the activation and reaction free energies. Finally we note that qualitatively similar free energy profiles are obtained at OM2/MM level, which also feature a shifted reactant minimum and increased $\Delta G^{\ddagger}$ and ΔG values for OM2/MM-DO compared with OM2/MM-ADD (Figure S1).

4.2 p-hydroxybenzoate hydroxylase

PHBH is a monooxygenase flavoprotein that catalyzes the conversion of p-hydroxybenzoate (pOHB) to 3,4-dihydroxybenzoate (DHB), a key step in the oxidative degradation process of aromatic compounds such as lignin.[1] The hydroxylation step in the PHBH catalytic cycle has been the focus of several theoretical studies.[55-60] In this step, an OH group with a formal charge of +1 migrates from the flavin-adenine hydroperoxide cofactor (FADHOOH) to the pOHB substrate (Scheme 2). The reaction involves considerable charge transfer and thus serves as an example, in which QM/MM calculations are expected to be responsive towards MM polarization.

We studied the PHBH-catalyzed hydroxylation reaction in a manner completely analogous to the CM-catalyzed reaction. We started from four randomly selected solvent-equilibrated snapshots of PHBH available from a previous study of our group.[53] In these snapshots, we modified the active site of PHBH by replacing the ribityl side chain of

FADHOOH with a methyl group. The QM region comprised pOHB and FADHOOH, with a total of 49 atoms. All atoms lying outside a residue-based cutoff of 10 Å from pOHB and FADHOOH were held fixed to their initial coordinates, and the non-bonded parameters of pOHB and FADHOOH were taken from the CHARMM22 force field. The PES scans were performed along a reaction coordinate that describes the OH transfer, namely the difference between the distances from the FADHOOH distal oxygen (O_d) to the proximal oxygen (O_p) and from the pOHB meta carbon (C_m) to O_d (Scheme 2).

$$z = d\left(O_d - O_p\right) - d\left(C_m - O_d\right)$$

The scans were performed with a grid spacing of 0.20 Å and, as in the case of CM, were carried out several times in the forward and backward directions, until the energies obtained from both directions were converged.

The ΔE and $\Delta E^{\ddagger}$ values of the PHBH-catalyzed reaction calculated using the DFT/MM-DO and DFT/MM-ADD models are listed in Table 3 for the four different snapshots; the corresponding potential energy profiles for snapshot 1 are illustrated in Figure 3A. Compared with DFT/MM-ADD, the energy barriers $\Delta E^{\ddagger}$ are consistently higher at the DFT/MM-DO level, by 1-4 kcal/mol for all four snapshots. On the other hand, the reaction free energies ΔE do not show such a trend: the DFT/MM-DO values are slightly lower (snapshots 1 and 4) or slightly higher (snapshots 2 and 3). Analogous OM2/MM results are reported in Table S3: here, inclusion of MM polarization at the OM2/MM-DO leads to an increase of the computed barriers $\Delta E^{\ddagger}$ for three out of four snapshots. The RMSDs between the DFT/MM-DO and DFT/MM-ADD optimized geometries of the corresponding stationary points for the various snapshots (Table S4) are typically higher than those observed in case of CM (Table S2) indicating that the effects

of MM polarization are more profound for PHBH than for CM.

Free energy profiles of the PHBH-catalyzed hydroxylation reaction calculated at the DFT/MM-DO and DFT/MM-ADD levels are shown in Figure 2B, and numerical results for free energies and geometric RMSDs are listed in Table 4. The profiles were determined by performing US simulations along the same reaction coordinate that had been used for the PES scans. As indicated in Figure 2B and Table 4, the free energy profiles exhibit trends that are largely consistent with those observed in the potential energy profiles. The activation free energy $\Delta G^{\ddagger}$ is significantly higher for the DFT/MM-DO model (18.2 kcal/mol) than for the DFT/MM-ADD model (13.7 kcal/mol), while the reaction free energy ΔG remains essentially unchanged between the two models (-47.1 vs. -46.9 kcal/mol)). The experimental $\Delta G^{\ddagger}$ value[55] is expected to be 14-15 kcal/mol,[59,61,62] which is closer the DFT/MM-ADD result. The geometric RMSDs between the average reactant, TS, and product structures sampled in the corresponding windows of the DFT/MM-DO and DFT/MM-ADD US simulations are typically much higher than those observed in the case of CM. Overlays of the corresponding DFT/MM-DO and DFT/MM-ADD average geometries (Figures 2C-2E) suggest that DFT/MM-DO favors an active site geometry in which pOHB and FADHOOH are closer to each other. The free energy profiles obtained at the OM2/MM level (Figure S2) show similar behavior as those obtained at the DFT/MM level (Figure 2B).

4.3 Computational aspects

Application of the QM/MM-DO model comes with a significant increase in computational expense. The computation times for single-point energy and gradient

evaluations at the QM/MM-DO and the QM/MM-ADD levels are compared in Table 5. Both in the case of CM and PHBH, DFT/MM-DO and OM2/MM-DO calculations are roughly 7 times and 11 times more expensive than the analogous DFT/MM-ADD and OM2/MM-ADD calculations, respectively. The reason for this large difference is that (a) in the current QM/MM-DO implementation, each QM/MM-DO step requires 5-6 SCF calculations to simultaneously converge the QM energy and the positions of the DPs, and (b) each SCF in the QM/MM-DO setup takes longer because of the presence of additional MM point charges that represent the DPs and LPs.

To put these timings into perspective, we note that the actual QM calculation takes a negligible amount of time in the case of OM2/MM-ADD. At the DFT/MM-ADD level, the QM calculation with external point charges takes more than 95% of the wall-clock time when using 20 cores; about a third of the computational effort is spent on evaluating the terms involving external point charges (see Table 5).

5. Discussion and Conclusions

In this article, we assessed the effects of MM polarization in QM/MM studies of enzymatic reactions by considering a polarizable QM/MM-DO model, in which the MM region is described by a DO-based polarizable force field. Using this model, we investigated the mechanisms of two well-studied enzymatic reactions, namely the CM-catalyzed chorismate-to-prephenate conversion and the PHBH-catalyzed hydroxylation reaction of p-hydroxybenzoate, by performing full geometry optimizations and free energy simulations. We generated potential energy and free energy profiles for these reactions and compared the results to those obtained from analogous calculations using

the traditional additive QM/MM-ADD model. We chose the recent CHARMM-DO force field for proteins and the SWM4 model for water to describe the polarizable MM atoms, and the CHARMM22 force field and TIP3 model for water to describe the additive MM atoms. The QM computations were performed at the reasonably robust B3LYP/def2-SVP level of theory. As a check for consistency, all calculations were repeated with the QM computations carried out at the semiempirical OM2 level. We emphasize that our conclusions on MM polarization effects are specific to the chosen force field representation and that analogous benchmarks should be performed also for other polarizable force fields to assess the general validity of our conclusions.

In case of CM, the potential energy profiles for the reaction obtained with the QM/MM-DO and QM/MM-ADD models were quite similar; the QM/MM-DO energy barriers and reaction energies for the five chosen snapshots were higher than the corresponding QM/MM-ADD values by 0.5-1.3 and 0.4-2.6 kcal/mol, respectively. This trend was highlighted in the corresponding free energy profiles. The QM/MM-DO free energy barrier and reaction free energy were higher than the corresponding QM/MM-ADD values by 2.5 and 2.9 kcal/mol, respectively. Upon close inspection of the geometries sampled during the QM/MM simulations, we observed that the QM/MM-DO and QM/MM-ADD simulations sample similar geometries in the transition state and product region, while the QM/MM-DO model favors a reactant geometry with a more open structure of the substrate and a slightly lower free energy, which accounts for the higher free energy barrier and reaction free energy (compared with QM/MM-ADD).

In an attempt to disentangle the effects of MM-DO polarization on the computed energies, we performed an energy decomposition analysis for each stationary point

obtained at the QM/MM-DO level for CM (see Supporting Information for the chosen procedure and detailed numerical results). We find that the effects of MM polarization on the computed QM energies are large in absolute terms, but they do not change much during the reaction (see Table S5). For example, as a consequence of compensating shifts, the inclusion of MM-DO polarization changes the QM energy of the transition state relative to the reactant typically by less than 1 kcal/mol (see Table S6).

For PHBH, the differences between the QM/MM-DO and QM/MM-ADD results were more pronounced than those observed in the case of CM. Both the potential energy and the free energy barriers calculated with QM/MM-DO were notably higher than those calculated with QM/MM-ADD, by 1.2-3.9 kcal/mol (four snapshots) and by 4.5 kcal/mol, respectively. The reaction energies and reaction free energies from QM/MM-DO and QM/MM-ADD showed no such clear trend and exhibited deviations in both directions.

In the CM- and PHBH-catalyzed reactions, MM polarization thus exerts the largest effect on the computed barrier in PHBH. This may be rationalized as follows. While the Claisen rearrangement in CM involves little charge transfer, the PHBH-catalyzed hydroxylation reaction requires the formal transfer of an OH^+ group from the neutral FADHOOH moiety to the pOHB dianion. The overall negative charge of -2 is fairly localized in the reactant state (pOHB dianion) and the product state (pOHB and FADHOOH anions), but rather delocalized between these two moieties in the transition state. The polarizable MM region will preferentially stabilize charge-localized states (reactant and product), which will in turn lead to an increase in the barrier.

To summarize, the present case study on the CM- and PHBH-catalyzed reactions has revealed moderate effects of MM polarization on activation and reaction (free)

energies. One obvious question is whether it is advisable in QM/MM studies of enzymatic reactions to move from the current QM/MM-ADD standard to the more refined QM/MM-DO level. Conventional QM/MM-ADD studies benefit from the availability of well-tested additive force fields, which should still be more robust than recently developed polarizable force fields, and they have the practical advantage of being much more efficient computationally (see the preceding section). On the other hand, MM polarization is a physical effect that exists and should in principle be included in QM/MM calculations that aim at high accuracy. In QM/MM studies of enzymatic reactions, the most important polarization effects on the energetics will arise from the region in and around the active site (since polarization effects in distant regions are expected to remain largely unchanged along a reaction pathway). An alternative way to include the leading polarization effects around the active site may be the use of larger QM regions in QM/MM-ADD calculations, which will account for important polarization contributions at the QM level. Given the significantly higher cost of QM/MM-DO compared with QM/MM-ADD, a moderate extension of the QM region would seem competitive in terms of computational effort, especially when using efficient linear scaling QM implementations. In view of these considerations, we believe that further validation work is required to establish the best QM/MM-based procedure for handling polarization effects in enzymatic reactions.

Supporting Information. Further numerical DFT/MM and OM2/MM results; free energy profiles from OM2/MM calculations; computational details and convergence behavior of string and US simulations; energy decomposition analysis.

Acknowledgement. This work was supported by an ERC Advanced Grant (OMSQC).

Schemes

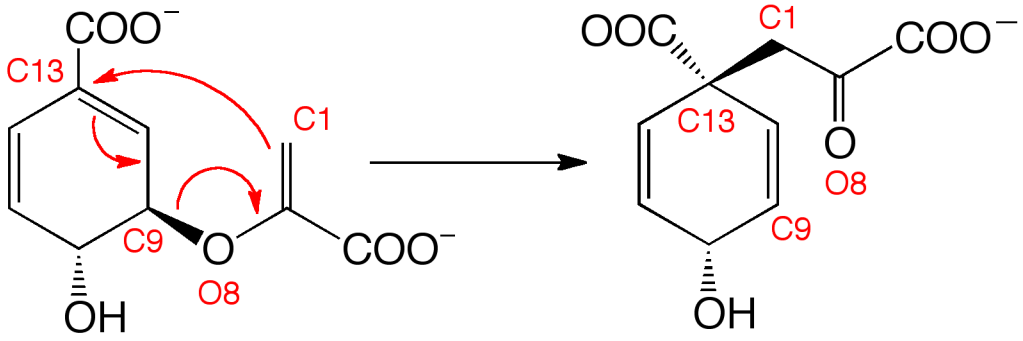

Scheme 1. Claisen rearrangement of chorismate to prephenate catalyzed by the chorismate mutase enzyme.

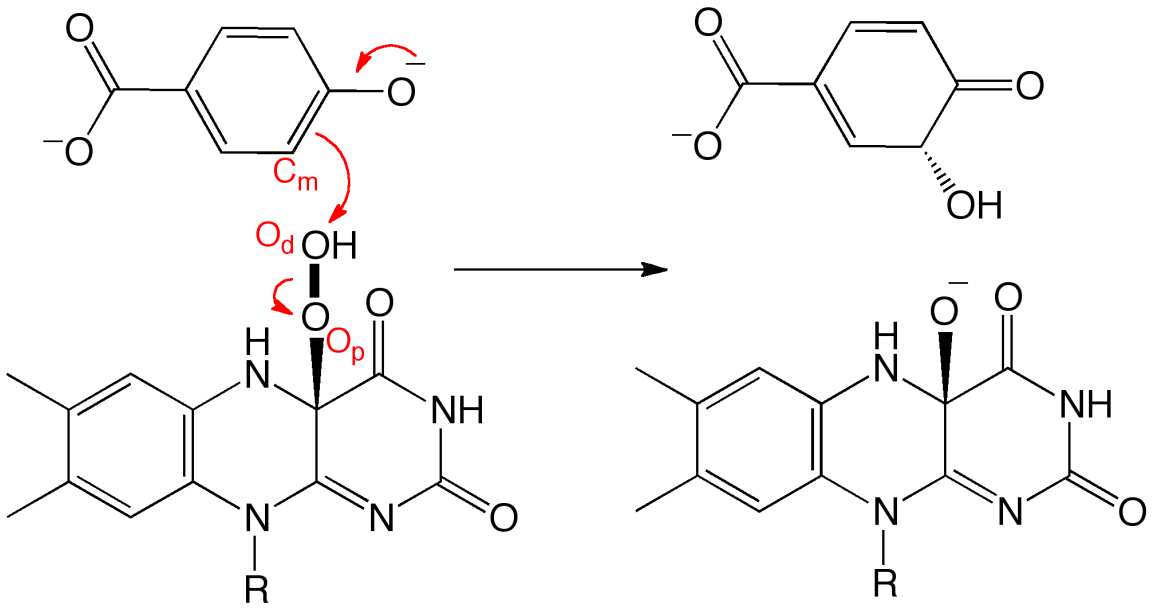

Scheme 2. Hydroxylation reaction catalyzed by the p-hydroxybenzoate hydrolase enzyme.

Figures

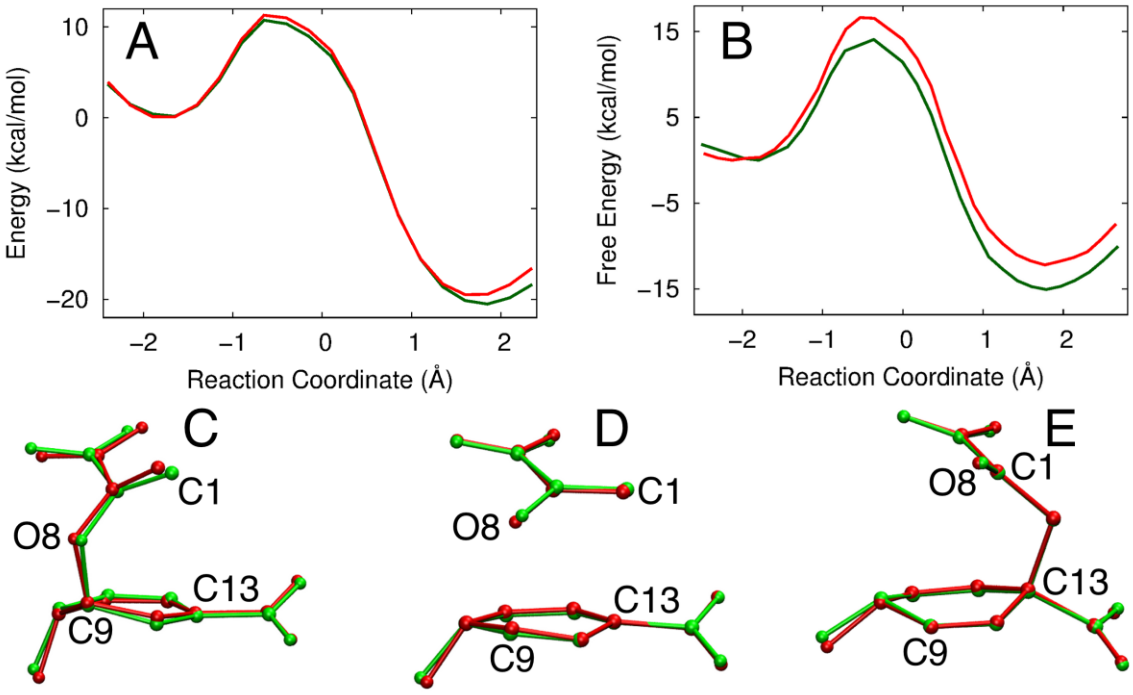

Figure 1. Investigation of the CM-catalyzed reaction using the QM/MM-DO and QM/MM-ADD models. Potential energy profiles (A) and free energy profiles (B) obtained using QM/MM-DO (red) and QM/MM-ADD (green) models. The potential energy profiles correspond to snapshot 1. Superimposition of the average reactant (C), transition state (D), and product (E) geometries sampled in the QM/MM-DO (red) and QM/MM-ADD (green) US simulations. The average reactant, transition state, and product geometries correspond to the mean structure sampled in the corresponding US simulation windows. The QM region was described at the B3LYP/def2-SVP level of theory.

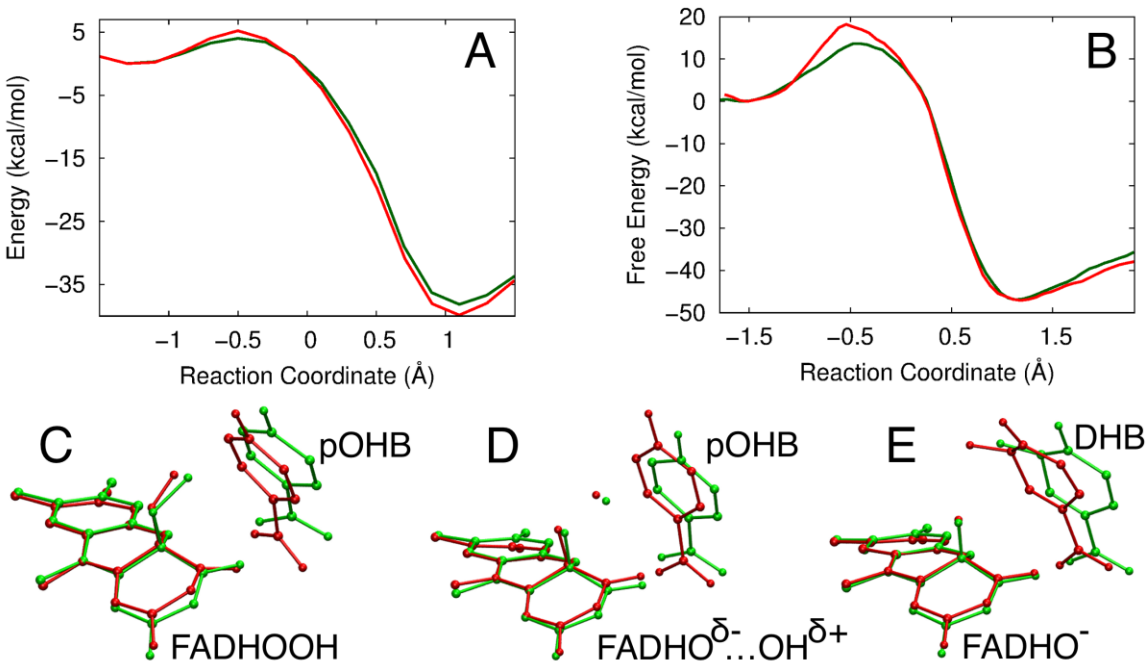

Figure 2. Investigation of the PHBH-catalyzed hydroxylation reaction using the QM/MM-DO and QM/MM-ADD models. Potential energy profiles (A) and free energy profiles (B) obtained using QM/MM-DO (red) and QM/MM-ADD (green) models. The potential energy profiles correspond to snapshot 1. Superimposition of the average reactant (C), transition state (D), and product (E) geometries sampled in the QM/MM-DO (red) and QM/MM-ADD (green) US simulations. The average reactant, transition state, and product geometries correspond to the mean structure sampled in the corresponding US simulation windows. In (C-E) the flavin-adenine hydroperoxide is labeled as FADHOOH, p-hydroxybenzoate is labeled as pOHB, and to 3,4-dihydroxybenzoate is labeled as DHB. The QM region was described at the B3LYP/def2-SVP level of theory.

Tables

Table 1. Reaction energies (ΔE) and activation energies ($\Delta E^{\ddagger}$) of the CM-catalyzed reaction for five snapshots with different initial configurations calculated using the QM/MM-DO and QM/MM-ADD models. The QM region was described at the B3LYP/def2-SVP level of theory. All values in kcal/mol.

	QM/MM-DO		QM/MM-ADD			
snapshot	ΔE	$\Delta E^{\ddagger}$	ΔE	$\Delta E^{\ddagger}$	$\Delta\Delta E$	$\Delta\Delta E^{\ddagger}$
1	-19.5	11.3	-20.6	10.8	1.1	0.5
2	-15.2	13.0	-15.2	13.4	0.0	-0.4
3	-11.3	17.7	-13.9	16.4	2.6	1.3
4	-15.9	14.1	-17.1	13.1	1.2	1.0
5	-17.9	11.6	-18.3	10.7	0.4	0.9
Mean	-16.0	13.5	-17.2	12.9	1.2	0.6

Table 2. Activation free energies, reaction free energies, and RMSDs of average reactant (R), transition state (TS), and product (P) geometries of the CM-catalyzed reaction obtained using the QM/MM-DO and QM/MM-ADD models at the (a) B3LYP/def2-SVP/MM and (b) OM2/MM levels of theory. The average R, TS, and P geometries correspond to the mean structure sampled in the corresponding US simulation windows. Free energies in kcal/mol and RMSDs in Å.

	QM/MM-DO		QM/MM-ADD				RMSD		
	ΔG	$\Delta G^{\ddagger}$	ΔG	$\Delta G^{\ddagger}$	$\Delta\Delta G$	$\Delta\Delta G^{\ddagger}$	R	TS	P
a	-12.2	16.6	-15.1	14.1	2.9	2.5	0.28	0.11	0.10
b	-16.9	20.1	-22.7	16.6	5.8	3.5	0.35	0.17	0.11

Table 3. Activation free energies, reaction free energies, and RMSDs of average reactant (R), transition state (TS), and product (P) geometries of the PHBH-catalyzed reaction obtained using the QM/MM-DO and QM/MM-ADD models. The average R, TS, and P geometries correspond to the mean structure sampled in the corresponding US simulation windows. The QM region was described at the B3LYP/def2-SVP level of theory. All values in kcal/mol.

	QM/MM-DO		QM/MM-ADD			
snapshot	ΔE	$\Delta E^{\ddagger}$	ΔE	$\Delta E^{\ddagger}$	$\Delta\Delta E$	$\Delta\Delta E^{\ddagger}$
1	-38.6	5.2	-38.2	4.0	-0.4	1.2
2	-35.5	11.0	-36.7	7.1	1.2	3.9
3	-38.2	5.4	-38.5	3.8	0.3	1.6
4	-41.4	5.3	-40.0	3.7	-1.4	1.6
Mean	-38.4	6.7	-38.4	4.7	-0.1	2.1

Table 4. Activation free energies, reaction free energies, and RMSDs of average reactant (R), transition state (TS), and product (P) geometries of the PHBH-catalyzed reaction obtained using the QM/MM-DO and QM/MM-ADD models at the (a) B3LYP/def2-SVP/MM and (b) OM2/MM levels of theory. The average R, TS, and P geometries correspond to the mean structure sampled in the corresponding US simulation windows. Free energies in kcal/mol and RMSDs in Å.

	QM/MM-DO		QM/MM-ADD				RMSD		
	ΔG	$\Delta G^{\ddagger}$	ΔG	$\Delta G^{\ddagger}$	$\Delta\Delta G$	$\Delta\Delta G^{\ddagger}$	R	TS	P
a	-47.1	18.2	-46.9	13.7	-0.2	4.5	0.52	0.59	0.76
b	-55.9	15.1	-53.0	9.0	-2.9	6.1	0.87	0.76	0.99

Table 5. Comparison of average computation times (in seconds) for the QM/MM-DO and QM/MM-ADD models. Timings are given for a single QM/MM energy and gradient evaluation at the (a) B3LYP/def2-SVP/MM and (b) OM2/MM levels of theory, and the average is taken over 10 independent calculations with different starting configurations. The DFT QM computations are parallelized over 20 cores (hardware: Intel Xeon E5-2690v2, 3.0 GHz, 64 GB RAM), while the OM2 QM and all other calculations are done on a single core (hardware: Intel Xeon X5570, 2.93 GHz). For comparison, please note the computation times for analogous gas-phase QM calculations: DFT (20 cores / 1 core), CM 21.8 / 222.5, PHBH 85.6 / 1358.8; OM2 (1 core), CM 0.08, PHBH 0.15.

System	Total atoms	QM atoms		Average time for computation		
				QM/MM-DO	QM/MM-ADD	Ratio
CM	13371	24	*a*	274.4	38.2	7.2
			b	52.2	4.4	11.9
PHBH	22716	49	*a*	1070.3	142.8	7.5
			b	159.3	13.9	11.5

References

(1) Senn, H. M.; Thiel, W. QM/MM Methods for Biomolecular Systems. *Angew. Chem. Int. Edit.* **2009**, *48*, 1198-1229.

(2) van der Kamp, M. W.; Mulholland, A. J. Combined Quantum Mechanics/Molecular Mechanics (QM/MM) Methods in Computational Enzymology. *Biochemistry* **2013**, *52*, 2708-2728.

(3) Brunk, E.; Rothlisberger, U. Mixed Quantum Mechanical/Molecular Mechanical Molecular Dynamics Simulations of Biological Systems in Ground and Electronically Excited States. *Chem. Rev.* **2015**, *115*, 6217-6263.

(4) Senn, H. M.; Thiel, W. QM/MM studies of enzymes. *Curr. Opin. Chem. Biol.* **2007**, *11*, 182-187.

(5) Lin, H.; Truhlar, D. G. QM/MM: what have we learned, where are we, and where do we go from here? *Theor Chem Acc* **2006**, *117*, 185-199.

(6) Shurki, A.; Warshel, A. Structure/Function Correlations of Proteins using MM, QM/MM, and Related Approaches: Methods, Concepts, Pitfalls, and Current Progress. In *Advances in Protein Chemistry*; Valerie, D., Ed.; Academic Press, 2003; Vol. 66; pp 249-313.

(7) Warshel, A.; Levitt, M. Theoretical studies of enzymic reactions: Dielectric, electrostatic and steric stabilization of the carbonium ion in the reaction of lysozyme. *J. Mol. Biol.* **1976**, *103*, 227-249.

(8) Kaminski, G. A.; Jorgensen, W. L. A Quantum Mechanical and Molecular Mechanical Method Based on CM1A Charges: Applications to Solvent Effects on Organic Equilibria and Reactions. *J. Phys. Chem. B* **1998**, *102*, 1787-1796.

(9) Kaminski, G. A.; Stern, H. A.; Berne, B. J.; Friesner, R. A. Development of an Accurate and Robust Polarizable Molecular Mechanics Force Field from ab Initio Quantum Chemistry. *J. Phys. Chem. A* **2004**, *108*, 621-627.

(10) Ren, P.; Ponder, J. W. Polarizable Atomic Multipole Water Model for Molecular Mechanics Simulation. *J. Phys. Chem. B* **2003**, *107*, 5933-5947.

(11) Ponder, J. W.; Wu, C.; Ren, P.; Pande, V. S.; Chodera, J. D.; Schnieders, M. J.; Haque, I.; Mobley, D. L.; Lambrecht, D. S.; DiStasio, R. A.; Head-Gordon, M.; Clark, G. N. I.; Johnson, M. E.; Head-Gordon, T. Current Status of the AMOEBA Polarizable Force Field. *J. Phys. Chem. B* **2010**, *114*, 2549-2564.

(12) Shi, Y.; Xia, Z.; Zhang, J.; Best, R.; Wu, C.; Ponder, J. W.; Ren, P. The Polarizable Atomic Multipole-based AMOEBA Force Field for Proteins. *J. Chem. Theory. Comput.* **2013**, *9*, 4046-4063.

(13) Patel, S.; Mackerell, A. D.; Brooks, C. L. CHARMM fluctuating charge force field for proteins: II Protein/solvent properties from molecular dynamics simulations using a nonadditive electrostatic model. *J. Comp. Chem.* **2004**, *25*, 1504-1514.

(14) Rappe, A. K.; Goddard, W. A. Charge equilibration for molecular dynamics simulations. *J Phys Chem-US* **1991**, *95*, 3358-3363.

(15) Stuart, S. J.; Berne, B. J. Effects of Polarizability on the Hydration of the Chloride Ion. *J Phys Chem-US* **1996**, *100*, 11934-11943.

(16) Lamoureux, G.; MacKerell, A. D.; Roux, B. t. A simple polarizable model of water based on classical Drude oscillators. *J. Chem. Phys.* **2003**, *119*, 5185-5197.

(17) Vorobyov, I.; Anisimov, V. M.; Greene, S.; Venable, R. M.; Moser, A.; Pastor, R. W.; MacKerell, A. D. Additive and Classical Drude Polarizable Force Fields for Linear and Cyclic Ethers. *J. Chem. Theory. Comput.* **2007**, *3*, 1120-1133.

(18) Jiang, W.; Hardy, D. J.; Phillips, J. C.; MacKerell, A. D.; Schulten, K.; Roux, B. High-Performance Scalable Molecular Dynamics Simulations of a Polarizable Force Field Based on Classical Drude Oscillators in NAMD. *J. Phys. Chem. Lett.* **2011**, *2*, 87-92.

(19) Yu, H.; Whitfield, T. W.; Harder, E.; Lamoureux, G.; Vorobyov, I.; Anisimov, V. M.; MacKerell, A. D.; Roux, B. Simulating Monovalent and Divalent Ions in Aqueous Solution Using a Drude Polarizable Force Field. *J. Chem. Theory. Comput.* **2010**, *6*, 774-786.

(20) Anisimov, V. M.; Lamoureux, G.; Vorobyov, I. V.; Huang, N.; Roux, B.; MacKerell, A. D. Determination of Electrostatic Parameters for a Polarizable Force Field Based on the Classical Drude Oscillator. *J. Chem. Theory. Comput.* **2005**, *1*, 153-168.

(21) Lamoureux, G.; Roux, B. Modeling induced polarization with classical Drude oscillators: Theory and molecular dynamics simulation algorithm. *J. Chem. Phys.* **2003**, *119*, 3025-3039.

(22) Illingworth, C. J. R.; Gooding, S. R.; Winn, P. J.; Jones, G. A.; Ferenczy, G. G.; Reynolds, C. A. Classical Polarization in Hybrid QM/MM Methods. *J. Phys. Chem. A* **2006**, *110*, 6487-6497.

(23) Illingworth, C. J. R.; Parkes, K. E.; Snell, C. R.; Marti, S.; Moliner, V.; Reynolds, C. A. The effect of MM polarization on the QM/MM transition state stabilization: application to chorismate mutase. *Mol Phys* **2008**, *106*, 1511-1515.

(24) Lopes, P. E. M.; Huang, J.; Shim, J.; Luo, Y.; Li, H.; Roux, B.; MacKerell, A. D. Polarizable Force Field for Peptides and Proteins Based on the Classical Drude Oscillator. *J. Chem. Theory. Comput.* **2013**, *9*, 5430-5449.

(25) Geerke, D. P.; Thiel, S.; Thiel, W.; van Gunsteren, W. F. QM-MM interactions in simulations of liquid water using combined semi-empirical/classical Hamiltonians. *Phys. Chem. Chem. Phys.* **2008**, *10*, 297-302.

(26) Boulanger, E.; Thiel, W. Solvent Boundary Potentials for Hybrid QM/MM Computations Using Classical Drude Oscillators: A Fully Polarizable Model. *J. Chem. Theory. Comput.* **2012**, *8*, 4527-4538.

(27) Boulanger, E.; Thiel, W. Toward QM/MM Simulation of Enzymatic Reactions with the Drude Oscillator Polarizable Force Field. *J. Chem. Theory. Comput.* **2014**, *10*, 1795-1809.

(28) Zhu, X.; Lopes, P. E. M.; MacKerell, A. D. Recent developments and applications of the CHARMM force fields. *WIREs Comput Mol Sci* **2012**, *2*, 167-185.

(29) Cornell, W. D.; Cieplak, P.; Bayly, C. I.; Gould, I. R.; Merz, K. M.; Ferguson, D. M.; Spellmeyer, D. C.; Fox, T.; Caldwell, J. W.; Kollman, P. A. A Second Generation Force Field for the Simulation of Proteins, Nucleic Acids, and Organic Molecules. *J. Am. Chem. Soc.* **1995**, *117*, 5179-5197.

(30) Kaminski, G. A.; Friesner, R. A.; Tirado-Rives, J.; Jorgensen, W. L. Evaluation and Reparametrization of the OPLS-AA Force Field for Proteins via

Comparison with Accurate Quantum Chemical Calculations on Peptides. *J. Phys. Chem. B* **2001**, *105*, 6474-6487.

(31) Thole, B. T. Molecular polarizabilities calculated with a modified dipole interaction. *Chem Phys* **1981**, *59*, 341-350.

(32) Harder, E.; Anisimov, V. M.; Vorobyov, I. V.; Lopes, P. E. M.; Noskov, S. Y.; MacKerell, A. D.; Roux, B. Atomic Level Anisotropy in the Electrostatic Modeling of Lone Pairs for a Polarizable Force Field Based on the Classical Drude Oscillator. *J. Chem. Theory. Comput.* **2006**, *2*, 1587-1597.

(33) Billeter, S. R.; Turner, A. J.; Thiel, W. Linear scaling geometry optimisation and transition state search in hybrid delocalised internal coordinates. *Phys. Chem. Chem. Phys.* **2000**, *2*, 2177-2186.

(34) Zhu, F.; Hummer, G. Pore opening and closing of a pentameric ligand-gated ion channel. *Proc. Natl. Acad. Sci. U.S.A.* **2010**, *107*, 19814-19819.

(35) Rosta, E.; Nowotny, M.; Yang, W.; Hummer, G. Catalytic mechanism of RNA backbone cleavage by ribonuclease H from quantum mechanics/molecular mechanics simulations. *J. Am. Chem. Soc.* **2011**, *133*, 8934-8941.

(36) Ganguly, A.; Thaplyal, P.; Rosta, E.; Bevilacqua, P. C.; Hammes-Schiffer, S. Quantum Mechanical/Molecular Mechanical Free Energy Simulations of the Self-Cleavage Reaction in the Hepatitis Delta Virus Ribozyme. *J. Am. Chem. Soc.* **2014**, *136*, 1483-1496.

(37) Zhang, S.; Ganguly, A.; Goyal, P.; Bingaman, J. L.; Bevilacqua, P. C.; Hammes-Schiffer, S. Role of the Active Site Guanine in the glmS Ribozyme Self-Cleavage Mechanism: Quantum Mechanical/Molecular Mechanical Free Energy Simulations. *J. Am. Chem. Soc.* **2015**, *137* 784-798.

(38) Lans, I.; Medina, M.; Rosta, E.; Hummer, G.; Garcia-Viloca, M.; Lluch, J. M.; González-Lafont, À. Theoretical Study of the Mechanism of the Hydride Transfer between Ferredoxin‚ÄìNADP+ Reductase and NADP+: The Role of Tyr303. *J. Am. Chem. Soc.* **2012**, *134*, 20544-20553.

(39) ChemShell, a Computational Chemistry Shell, see http://www.chemshell.org.

(40) Sherwood, P.; de Vries, A. H.; Guest, M. F.; Schreckenbach, G.; Catlow, C. R. A.; French, S. A.; Sokol, A. A.; Bromley, S. T.; Thiel, W.; Turner, A. J.; Billeter, S.; Terstegen, F.; Thiel, S.; Kendrick, J.; Rogers, S. C.; Casci, J.; Watson, M.; King, F.; Karlsen, E.; Sjøvoll, M.; Fahmi, A.; Schäfer, A.; Lennartz, C. QUASI: A general purpose implementation of the QM/MM approach and its application to problems in catalysis. *Journal of Molecular Structure: THEOCHEM* **2003**, *632*, 1-28.

(41) Metz, S.; Kästner, J.; Sokol, A. A.; Keal, T. W.; Sherwood, P. ChemShell—a modular software package for QM/MM simulations. *WIREs Comput Mol Sci* **2014**, *4*, 101-110.

(42) Becke, A. D. A new mixing of Hartree–Fock and local density-functional theories. *J. Chem. Phys.* **1993**, *98*, 1372-1377.

(43) Becke, A. D. Density-functional thermochemistry. III. The role of exact exchange. *J. Chem. Phys.* **1993**, *98*, 5648-5652.

(44) Schäfer, A.; Horn, H.; Ahlrichs, R. Fully optimized contracted Gaussian basis sets for atoms Li to Kr. *J. Chem. Phys.* **1992**, *97*, 2571-2577.

(45) Weber, W.; Thiel, W. Orthogonalization corrections for semiempirical methods. *Theor Chem Acc* **2000**, *103*, 495-506.

(46) Dral, P. O.; Wu, X.; Spörkel, L.; Koslowski, A.; Thiel, W. Semiempirical Quantum-Chemical Orthogonalization-Corrected Methods: Benchmarks for Ground-State Properties. *J. Chem. Theory. Comput.* **2016**, *12*, 1097-1120.

(47) Dral, P. O.; Wu, X.; Spörkel, L.; Koslowski, A.; Weber, W.; Steiger, R.; Scholten, M.; Thiel, W. Semiempirical Quantum-Chemical Orthogonalization-Corrected Methods: Theory, Implementation, and Parameters. *J. Chem. Theory. Comput.* **2016**, *12*, 1082-1096.

(48) Ahlrichs, R.; Bär, M.; Häser, M.; Horn, H.; Kölmel, C. Electronic structure calculations on workstation computers: The program system turbomole. *Chem. Phys. Lett.* **1989**, *162*, 165-169.

(49) Thiel, W. MNDO2004 Max-Planck-Institut für Kohlenforschung; Mülheim an der Ruhr, Germany, 2004, 2004.

(50) Forrester, T. R.; Smith, W. DL-POLY program;Daresbury Laboratory: Daresbury, Warrington, England, 1996.

(51) MacKerell, A. D.; Bashford, D.; Bellott, M.; Dunbrack, R. L.; Evanseck, J. D.; Field, M. J.; Fischer, S.; Gao, J.; Guo, H.; Ha, S.; Joseph-McCarthy, D.; Kuchnir, L.; Kuczera, K.; Lau, F. T. K.; Mattos, C.; Michnick, S.; Ngo, T.; Nguyen, D. T.; Prodhom, B.; Reiher, W. E.; Roux, B.; Schlenkrich, M.; Smith, J. C.; Stote, R.; Straub, J.; Watanabe, M.; Wiórkiewicz-Kuczera, J.; Yin, D.; Karplus, M. All-Atom Empirical Potential for Molecular Modeling and Dynamics Studies of Proteins. *J. Phys. Chem. B* **1998**, *102*, 3586-3616.

(52) Lamoureux, G.; Harder, E.; Vorobyov, I. V.; Roux, B.; MacKerell Jr, A. D. A polarizable model of water for molecular dynamics simulations of biomolecules. *Chem. Phys. Lett.* **2006**, *418*, 245-249.

(53) Benighaus, T.; Thiel, W. Long-Range Electrostatic Effects in QM/MM Studies of Enzymatic Reactions: Application of the Solvated Macromolecule Boundary Potential. *J. Chem. Theory. Comput.* **2011**, *7*, 238-249.

(54) Kast, P.; Hartgerink, J. D.; Asif-Ullah, M.; Hilvert, D. Electrostatic Catalysis of the Claisen Rearrangement: Probing the Role of Glu78 in Bacillus subtilis Chorismate Mutase by Genetic Selection. *J. Am. Chem. Soc.* **1996**, *118*, 3069-3070.

(55) Senn, H. M.; Thiel, S.; Thiel, W. Enzymatic Hydroxylation in p-Hydroxybenzoate Hydroxylase: A Case Study for QM/MM Molecular Dynamics. *J. Chem. Theory. Comput.* **2005**, *1*, 494-505.

(56) Claeyssens, F.; Harvey, J. N.; Manby, F. R.; Mata, R. A.; Mulholland, A. J.; Ranaghan, K. E.; Schütz, M.; Thiel, S.; Thiel, W.; Werner, H.-J. High-Accuracy Computation of Reaction Barriers in Enzymes. *Angew. Chem. Int. Ed.* **2006**, *45*, 6856-6859.

(57) Mata, R. A.; Werner, H.-J.; Thiel, S.; Thiel, W. Toward accurate barriers for enzymatic reactions: QM/MM case study on p-hydroxybenzoate hydroxylase. *J. Chem. Phys.* **2008**, *128*, 025104-025108.

(58) Billeter, S. R.; Hanser, C. F. W.; Mordasini, T. Z.; Scholten, M.; Thiel, W.; van Gunsteren, W. F. Molecular dynamics study of oxygenation reactions catalysed by the enzyme p-hydroxybenzoate hydroxylase. *Phys. Chem. Chem. Phys.* **2001**, *3*, 688-

695.

(59) Ridder, L.; Mulholland, A. J.; Rietjens, I. M. C. M.; Vervoort, J. A Quantum Mechanical/Molecular Mechanical Study of the Hydroxylation of Phenol and Halogenated Derivatives by Phenol Hydroxylase. *J. Am. Chem. Soc.* **2000**, *122*, 8728-8738.

(60) Ridder, L.; Harvey, J. N.; Rietjens, I. M. C. M.; Vervoort, J.; Mulholland, A. J. Ab Initio QM/MM Modeling of the Hydroxylation Step in p-Hydroxybenzoate Hydroxylase. *J. Phys. Chem. B* **2003**, *107*, 2118-2126.

(61) Van Berkel, W. J. H.; Müller, F. The temperature and pH dependence of some properties of p-hydroxybenzoate hydroxylase from Pseudomonas fluorescens. *Eur J Biochem* **1989**, *179*, 307-314.

(62) Vervoort, J.; Rietjens, I. M. C. M.; van Berkel, W. J. H.; Veeger, C. Frontier orbital study on the 4-hydroxybenzoate-3-hydroxylase-dependent activity with benzoate derivatives. *Eur J Biochem* **1992**, *206*, 479-484.

TOC Graphic

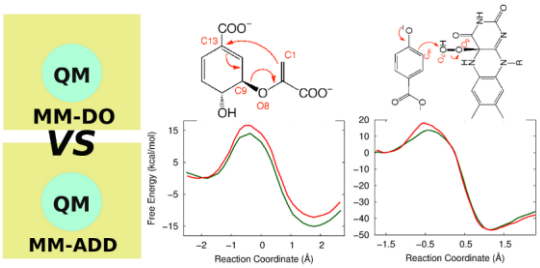
QM
MM-DO
VS
QM
MM-ADD
COO⁻
C13
C1
C9
O8
COO⁻
OH
Free Energy (kcal/mol)
Reaction Coordinate (Å)
Reaction Coordinate (Å)